Optical coherence-based techniques for motional Stark effect measurements of magnetic field pitch angle

1999 Plasma Phys. Control. Fusion 41 271

(http://iopscience.iop.org/0741-3335/41/2/012)

Plasma Phys. Control. Fusion **41** (1999) 271–284. Printed in the UK PII: S0741-3335(99)88859-9

Optical coherence-based techniques for motional Stark effect measurements of magnetic field pitch angle

John Howard

Plasma Research Laboratory, Australian National University, Canberra ACT 0200, Australia

Received 28 October 1997, in final form 24 November 1998

Abstract. The motional Stark effect measurement of magnetic field pitch angle in tokamaks is a mature and powerful technique for estimating plasma current density in tokamaks. However, its range of applicability is limited by the requirement that σ and π manifolds are spectrally sufficiently well separated (high magnetic fields, high beam energies) to ensure adequate net polarization for a successful measurement. This paper proposes alternative schemes based on the optical coherence properties of the Stark multiplet that are somewhat more versatile than the standard method and better suited to measurements on low-field toroidal confinement devices. An interference filter is used to transmit the Stark multiplet to a polarimeter (which uses a single photoelastic plate) that modulates the light temporal coherence and/or its first spectral moment. This light is subsequently processed using a novel electro-optically modulated solid-state interferometer that is sensitive to low-order spectral moments. The modulation of these quantities conveys information about the orientation of the light polarization and hence the magnetic field pitch angle.

1. Introduction

The recent interest in boostrap-current sustained compact tokamaks as alternative fusion devices has highlighted the need for accurate measurements of magnetic field strength and pitch angle. Motional Stark effect (MSE) polarimetry is now a standard diagnostic for estimating the magnetic field pitch angle in tokamaks using high-power heating beams [1–4]. However, its extension to low-field compact systems such as the NSTX spherical tokamak is problematic because of the much smaller expected Stark spectral shifts.

The MSE technique relies on the splitting of the high-energy neutral beam Balmer α light into orthogonally polarized σ and π components as a result of the motion-induced strong electric field $\boldsymbol{E} = \boldsymbol{v} \times \boldsymbol{B}$ experienced in the rest frame of the neutral atoms. When viewed in a direction perpendicular to $\boldsymbol{E}$ the Stark split σ and π components are polarized, perpendicular and parallel to the direction of $\boldsymbol{E}$ respectively. When viewed along $\boldsymbol{E}$ the σ components are unpolarized and the π components have no intensity. The magnetic field pitch angle is usually estimated by isolating and measuring the polarization direction of the central cluster of σ lines.

The Stark separation of adjacent spectral components is given by $\Delta\lambda_S = 2.7574 \times 10^{-8} E$ nm where $E = |\boldsymbol{v} \times \boldsymbol{B}|$ is the induced electric field [5]. The required separation of σ and π clusters strongly constrains the range of beam energies, energy spreads and magnetic fields for which the method is useful [5, 6]. The primary reason for this is that the heating beam divergence Doppler broadens the Stark components so that at low magnetic fields ($\sim$1 T) the σ and π components can no longer be easily separated. The greater Stark separation of Balmer β lines is offset by their lower intensity.

0741-3335/99/020271+14$19.50

To alleviate these problems, we propose here an alternative measurement scheme that uses a simpler polarimeter for modulating the polarization of the Stark multiplet. The polarimeter output is combined with an electro-optically modulated solid-state spectrometer (MOSS) that is sensitive to the temporal coherence of the Stark spectrum and so is complementary in nature to the frequency domain narrowband filters usually applied to isolate central σ components. The MOSS spectrometer has been developed specifically to measure the low order spectral moments of line emission from optically thin radiant media [7, 8]. By modulating the polarization state of the input light, the MOSS spectrometer discriminates between emission from the spectrally separated and orthogonally polarized σ and π components by sensing the associated variations in net coherence of the light transmitted through an analyser. The new method is simple to implement, and potentially increases the useful operating range for the diagnostic.

The paper is organized as follows. In section 2 we describe a spherical quadrature polarimeter based on two birefringent plates and an analyser that enables simultaneous determination of the three Stokes parameters. As applied to MSE measurements, the instrument differs from the standard polarimetric technique [2] in that it requires only a single photoelastic modulator (PEM [9]) and a quarter waveplate. The light is subsequently processed by the MOSS spectrometer which is described briefly in section 3. Results of simulations are presented in section 4 and their application to magnetic field pitch angle measurements in low-field tokamaks is considered.

2. Polarimeter

The polarimeter uses two birefringent phase plates (delays δ_1 and δ_2) having their fast axes mutually oriented at 45°. The plates are followed by an analyser oriented to transmit light polarized parallel to the fast axis of the first phase plate (the x direction). The intensity of the light transmitted (or reflected) by the analyser is related to the Stokes vector of the input radiation by [10]

$$P = \frac{I}{2}(1 \pm \boldsymbol{s} \cdot \boldsymbol{p}) \tag{1}$$

$$\boldsymbol{s} = (\cos 2\psi \cos 2\epsilon, \sin 2\psi \cos 2\epsilon, \sin 2\epsilon) \tag{2}$$

$$\boldsymbol{p} = (\cos \delta_2, \sin \delta_2 \sin \delta_1, \sin \delta_2 \cos \delta_1) \tag{3}$$

where $\boldsymbol{s}$ is the Stokes vector and ψ and ϵ are the tilt angle with respect to the x axis and the ellipticity of the vibrational ellipse, respectively. Equations (2) and (3) represent points on the Poincaré sphere. Accordingly it is clear that if the phase plates are replaced by PEMs operating at frequencies Ω_1 and Ω_2 it is possible, using appropriate delay amplitudes and synchronous detection techniques to measure simultaneously all the components of $\boldsymbol{s}$.

The standard MSE polarimeter differs from these in that the final analyser is oriented at 22.5° to each of the PEM modulators and the ellipse tilt angle ψ is encoded as amplitude modulations $\sin 2\psi$ and $\cos 2\psi$ at the PEM modulation frequencies Ω_1 and Ω_2, respectively. The polarimeter proposed here (see figure 1) requires a quarter waveplate ($\delta_1 = \pi/2$) and a single modulator ($\delta_2 = \delta \sin \Omega_P t$ with modulation amplitude $\delta = \pi/2$). Using equation (1) it is straightforward to obtain the transmitted polarimeter signal as

$$\begin{aligned} P(\lambda) &= P_\sigma(\lambda) + P_\pi(\lambda) \\ 2P_\sigma(\lambda) &= \mathcal{I}_\sigma(1 + \cos 2\psi \cos 2\epsilon_\sigma \cos \delta_2 + \sin 2\psi \cos 2\epsilon_\sigma \sin \delta_2) \\ 2P_\pi(\lambda) &= \mathcal{I}_\pi(1 - \cos 2\psi \cos 2\epsilon_\pi \cos \delta_2 - \sin 2\psi \cos 2\epsilon_\pi \sin \delta_2) \end{aligned} \tag{4}$$

where the ellipse axes for σ and π components are taken as orthogonal and we allow the intensities and ellipticities to be functions of wavelength. The intensities $P_\pi(\lambda)$ and $P_\sigma(\lambda)$ are

the wavelength dependent intensities from the π and σ manifolds, respectively. These can be combined to give for the intensity at the two polarimeter ports

$$2P_{\pm}(\lambda) = \mathcal{I}(\lambda)(1 \pm \zeta_{\mathrm{P}}(\lambda)\cos(2\psi - \delta \sin \Omega_{\mathrm{P}} t)) \tag{5}$$

where $\mathcal{I} = \mathcal{I}_{\sigma} + \mathcal{I}_{\pi}$ is the total intensity and

$$\zeta_{\mathrm{P}} = \frac{\mathcal{I}_{\sigma} \cos 2\epsilon_{\sigma} - \mathcal{I}_{\pi} \cos 2\epsilon_{\pi}}{\mathcal{I}_{\sigma} + \mathcal{I}_{\pi}} \tag{6}$$

is the net polarization 'contrast'. The ellipticity terms account, for example, for contributions from Zeeman splitting, the unpolarized σ light due to the component of $\boldsymbol{E}$ in the direction of view and linear birefringence of optical windows and mirrors in the light path to the polarimeter. Though the ellipticity acts to reduce the polarization contrast, the sign of the ellipticity is of no consequence for the relative phase of P_{σ} and P_{π} components. In the interest of notational simplicity, we take $\epsilon_{\sigma} = \epsilon_{\pi} = 0$ in the remainder of this paper. Clearly, the oscillation $\delta \sin \Omega_{\mathrm{P}} t$ modulates the transmitted light intensity according to its polarization properties.

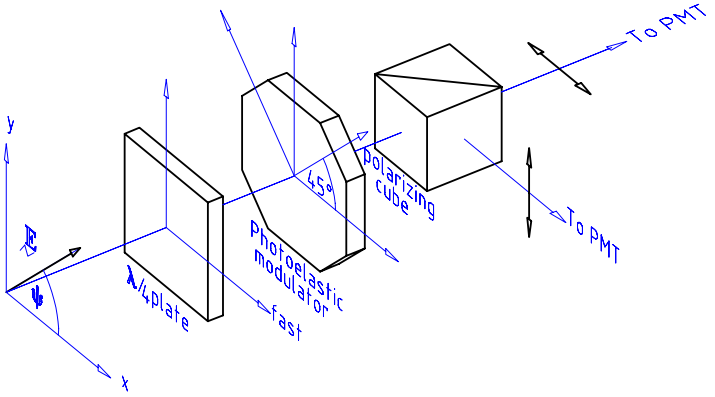

Figure 1. The layout for the proposed MSE polarimeter.

For a given wavelength, and provided the polarization contrast is sufficiently great, the polarimeter signals will give the quadrature components $\sin 2\psi$ and $\cos 2\psi$ at Ω_{P} and $2\Omega_{\mathrm{P}}$, respectively. An alternative digital demodulation scheme, however, is to sample the signals $P_{\pm}(\lambda)$ at times $t = nT/4$, $n = 0, 1, 2, \ldots$, $T = 2\pi/\Omega$, to record directly the components

$$\begin{aligned} 2P_{0\pm} &= \mathcal{I}(1 \pm \zeta_{\mathrm{P}} \cos 2\psi) \\ 2P_{1\pm} &= \mathcal{I}(1 \mp \zeta_{\mathrm{P}} \sin 2\psi) \\ 2P_{2\pm} &= 2P_{0\pm} \\ 2P_{3\pm} &= \mathcal{I}(1 \pm \zeta_{\mathrm{P}} \sin 2\psi). \end{aligned} \tag{7}$$

After re-synchronizing the quadrature sampled signals, the polarization tilt angle can be extracted without the loss of signal energy associated with lock-in techniques that track only a single harmonic component. The demodulation algorithm, which has been used routinely for the MOSS spectrometer is described more fully in [7].

Since the spectrally integrated intensities for σ and π components are comparable [11], some spectral discrimination is required to enhance the polarization contrast. The standard approach is to isolate σ components using a narrowband interference filter. This is satisfactory provided the Stark splitting $\Delta\lambda_{\mathrm{S}}$ is sufficiently large for the π components to fall substantially outside the filter passband $\Delta\lambda_{\mathrm{F}}$. In addition, it is also necessary that the splitting be large or

comparable to the spectral broadening $\Delta\lambda_B$ of the line due to the neutral beam divergence. These two conditions limit the range of beam energies and magnetic field strengths for which the method is useful.

3. Modulated solid-state spectrometer

The modulated solid-state spectrometer has been used for flow velocity and ion temperature measurements on the H-1 NF heliac at the Australian National University [12]. The principle of the spectrometer is illustrated in figure 2. The temporal coherence of an isolated spectral line (inverse of spectral bandwidth) is estimated using two-beam interferometric techniques. Changes in fringe visibility owing to variations in the temporal coherence of the light are visualized by electro-optically modulating the interferometric phase about some fixed offset phase delay. Simultaneously, variations in the first spectral moment of the emission (for example, a bulk motion-induced Doppler shift of the line centre frequency) causes an effective change in the fixed delay offset (accordion effect) that is registered as a variation in the relative intensities of the modulation harmonics.

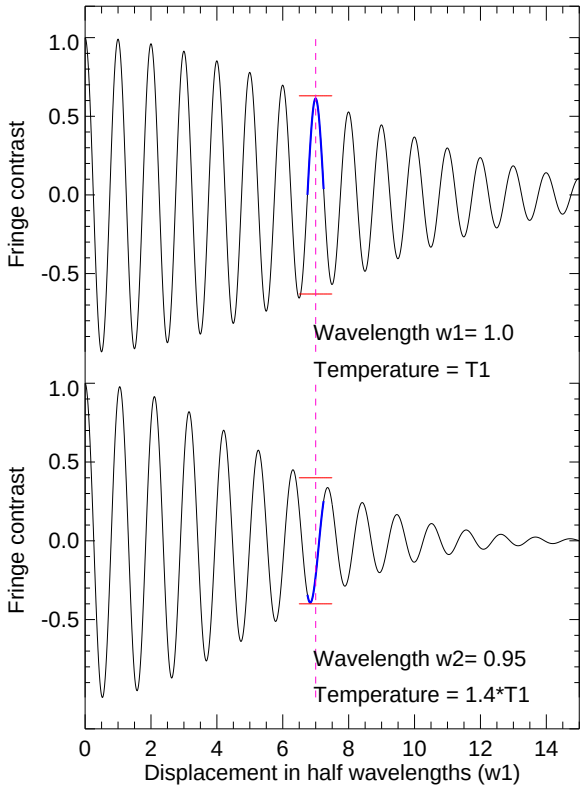

Figure 2. Simulated interferograms showing the effect on the interferogram phase of a change in line centre frequency (exaggerated for clarity). The broken vertical line corresponds to the delay introduced by the birefringent crystal while the bold section is the portion of the interferogram swept by the delay modulation. Wavelength changes are conveyed by the change in the ratio of even and odd harmonics generated by the modulation. The decrease in fringe contrast (horizontal bars) can be related to the temperature of the emitting species.

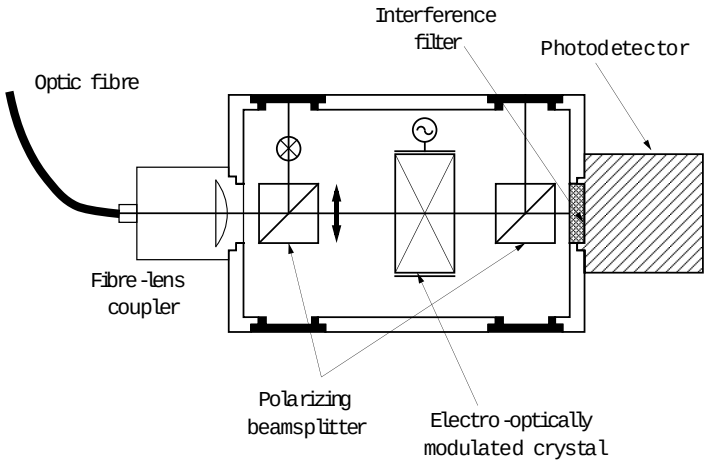

Figure 3. The optical layout for the modulated solid-state spectrometer.

The physical implementation of the device is shown in Figure 3. Light at wavelength λ is transmitted by a narrowband interference filter before being polarized using a broadband polarizing beamsplitter cube. The transmitted light then traverses a birefringent crystal of thickness L ($LiNbO_3$, birefringence $B = -0.1$) whose fast axis is at 45° to the plane of polarization. This introduces the fixed offset phase delay

$$\phi = 2\pi BL/\lambda \tag{8}$$

between the orthogonal characteristic waves. An additional small delay modulation $\phi_M \sin(\Omega_M t)$ of amplitude $\phi_M = \pi/2$ is imposed by applying an oscillating voltage of amplitude ~1000 V along the crystal z-axis. Provided the applied electro-optic modulation is far from the crystal mechanical resonances, the phase delay is uniform across the crystal face. Finally, the light is once more polarized using a beamsplitter cube to allow the independent components to interfere at photomultiplier tubes intercepting the transmitted and reflected beams.

We are interested in the instrument response to emission from a localized region defined by the intersection of the viewing line of sight (characterized by unit vector $\hat{\boldsymbol{l}}$) and the heating beam source and will ignore the effects of spatial integration. We model the nth beam emission line component for the σ manifold as

$$\mathcal{I}_\sigma^{(n)}(\lambda;\hat{\boldsymbol{l}}) = \frac{I_\sigma^{(n)}}{\sqrt{2\pi}\,\Delta\lambda_B}\exp\left(-\frac{(\lambda-\lambda_n)^2}{2\Delta\lambda_B^2}\right) \tag{9}$$

where $I_\sigma^{(n)}$ is the emission intensity, $\lambda_n = \lambda_{0n}(1-\beta_B)$, $\beta_B = \boldsymbol{v}_B\cdot\hat{\boldsymbol{l}}/c$ is the Doppler shifted emission line centre, $\lambda_{0n} = \lambda_0 + n\Delta\lambda_S$ is the rest frame centre wavelength for the nth Stark component and $\boldsymbol{v}_B$ is the beam velocity. The line width $\Delta\lambda_B$ is determined by the projection of the beam velocity spread onto $\hat{\boldsymbol{l}}$. For simplicity we assume the profile is Gaussian with equivalent temperature given by $kT_B/(m_Bc^2) = (\Delta\lambda_B/\lambda_0)^2$ where m_B is the atomic weight of the beam species.

The MOSS spectrometer output signal is the same as that for a Fourier transform spectrometer with path length delay $\phi_n + \phi_M \sin\Omega_M t$ where $\phi_n = 2\pi BL(1+\beta_B)/\lambda_n$ is the phase offset introduced by the birefringent plate. For the nth σ line the signals $S_{\sigma\pm}^{(n)}$ at the two output ports of the spectrometer are given by

$$2S_{\sigma\pm}^{(n)} = I_\sigma^{(n)}(1 \pm \zeta_B\cos(\phi_n + \phi_M\sin\Omega_M t)). \tag{10}$$

Because the polarimeter is also effectively a dual beam interferometer, it is not surprising that equation (5) has the same form as equation (10) but with fringe visibility ζ_B related to the species temperature T_B by

$$\zeta_B = \exp(-T_B/T_C) \tag{11}$$

where the 'characteristic temperature' of the birefringent crystal

$$T_C = \frac{2m_B c^2}{k\phi_0^2} \tag{12}$$

is determined by the delay ϕ_0. Because $n\Delta\lambda_S/\lambda_0 \ll 1$, it is an excellent approximation to take the spectral contrast, or fringe visibility ζ_B to be independent of the line index n. When $T_B = T_C$ we obtain $\phi_0 = \sqrt{2}(\lambda_0/\Delta\lambda_B)$ so that the phase delay ϕ_0 is a direct measure of the instrument resolving power.

The spectrometer response to the $\mathcal{I}_\sigma(\lambda)$ manifold is obtained by summing over the component transitions to obtain

$$2S_{\sigma\pm} = I_\sigma(1 \pm \zeta_\sigma \cos(\phi_0 + \phi_M \sin\Omega_M t)) \tag{13}$$

with

$$I_\sigma = 2{\sum_{n\geqslant 0}}' I_\sigma^{(n)} \tag{14}$$

$$\zeta_\sigma = \frac{\zeta_B}{I_\sigma}\left(2{\sum_{n\geqslant 0}}' I_\sigma^{(n)} \cos\left(\phi_0 n \frac{\Delta\lambda_S}{\lambda_0}\right)\right) \tag{15}$$

where the primed sum indicates that the $n = 0$ term is to be halved. An analogous expression can be written down for the π group but with different intensities and shifts. The cosine term within brackets represents an effective decrease in fringe contrast attending the broadening of the σ manifold due to the Stark shift of the $n \neq 0$ components from λ_0. The relative importance of the Stark separation $\Delta\lambda_S$ and the beam broadening $\Delta\lambda_B$ for the overall fringe visibility is determined by the resolving power through the choice of phase offset ϕ_0. Note that for small Stark shifts, the change of fringe contrast depends *quadratically* on the Stark shift $\Delta\lambda_S$.

4. MSE diagnostic

4.1. Contrast modulation

The polarimeter transmits alternately π and σ manifolds using polarization modulation techniques at frequency Ω_P. Since the spectral bandwidth of the π manifold is greater than for the central σ components, the spectrometer can enhance the signal modulation depth given an appropriate choice of phase delay ϕ_0. The response, however, is also sensitive to this choice through the carrier phase $\phi_0 + \phi_M \sin\Omega_M t$. It is, therefore, necessary to choose a MOSS modulation frequency Ω_M that is sufficiently high compared with Ω_P, so that the polarimetric modulation appears as an amplitude modulation of the carrier at Ω_M. The total system response is constructed by combining equation (13) and its π manifold equivalent with equation (5) for the light transmitted by the polarimeter:

$$\begin{aligned} 2T_\pm = {} & (I_\sigma \cos^2(\tilde{\psi}) + I_\pi \sin^2(\tilde{\psi})) \\ & \pm (I_\sigma \zeta_\sigma \cos^2(\tilde{\psi}) + I_\pi \zeta_\pi \sin^2(\tilde{\psi})) \cos(\tilde{\phi}) \end{aligned} \tag{16}$$

where $\tilde{\psi} = \psi - (\delta/2)\sin\Omega_P t$ is the modulated polarimetric phase and $\tilde{\phi} = \phi_0 - \phi_M \sin\Omega_M t$ is the modulated interferometric phase. Note that, in combining the polarimeter and spectrometer,

the need for the final polarimeter analysing cube is eliminated. This can be seen in figure 4. Signal to noise ratios can be improved by taking *both* transmitted and reflected signals via optical fibres to photomultiplier tubes remote from the magnetic field.

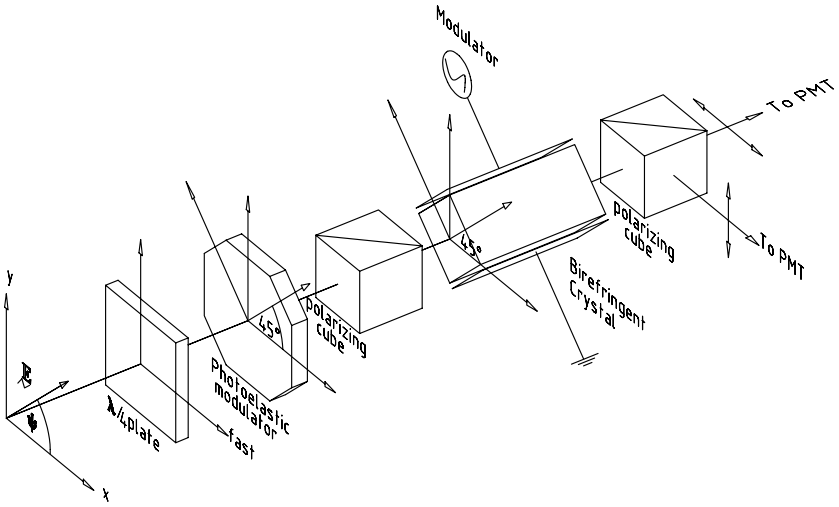

Figure 4. A schematic diagram of the combined polarimeter and MOSS spectrometer arrangement necessary for contrast modulation MSE measurements.

In order to emphasize the measurement principle, we make the reasonable simplifying approximation that the total intensities of σ and π manifolds are comparable [11], i.e. $I_\sigma = I_\pi \equiv I_0$. This gives

$$\frac{2T_\pm}{I_0} = 1 \pm (\zeta_\sigma \cos^2(\tilde{\psi}) + \zeta_\pi \sin^2(\tilde{\psi})) \cos(\tilde{\phi}). \tag{17}$$

The modulation $\tilde{\psi}$ transmits alternately the different polarization states of the Stark multiplet. The difference in their associated spectral widths results in a modulation of the fringe contrast of amplitude $\zeta_\mathrm{T} = (\zeta_\sigma - \zeta_\pi)/2$. The relative intensities of the fundamental and second-harmonic components of the contrast modulation gives the information about the polarization alignment ψ. The quantity $I_0\zeta_\mathrm{T}$ is the maximum absolute modulation amplitude of the light intensity and depends on the magnetic field strength. Changes in the phase ϕ_0 of the carrier at Ω_M reveal changes in the beam induced Doppler shift or spectral asymmetries.

If information about the interferometric phase ϕ is not required, a simpler 'homodyne scheme is obtained by setting the phase $\tilde{\phi} = 0$. This is achieved by applying an appropriate dc bias voltage to the MOSS birefringent plate. In this case, only the polarimetric contrast modulation survives and a synchronous sampling demodulation scheme such as that suggested by equation (7) will give directly the polarization tilt. This also overcomes the practical difficulty of having to provide an electro-optically generated carrier at frequencies significantly higher than the first PEM modulator frequency (typically 40 kHz).

Because $\zeta_\pi < \zeta_\sigma < 1$ the polarization contrast (i.e. modulation depth at Ω_P) can be maximized by an appropriate choice of delay ϕ_0. To illustrate this we have simulated the response of the proposed polarimeter/MOSS spectrometer system and compared this with the filter spectrometer technique. We have assumed a deuterium heating beam of energy 50 keV and temperature $T_\mathrm{B} = 10$ eV equivalent to a beam divergence of 0.8° and spectral width $\Delta\lambda_\mathrm{B} = 0.048$ nm for a viewing line at angle 45° to the beam (blue-shifted). For simplicity,

we ignore the solid angle of the light-collecting optics. The model MSE spectra calculated for fields 0.5 T and 1.5 T are shown in figure 5. It has been assumed that an interference filter preselects only the full energy emission components.

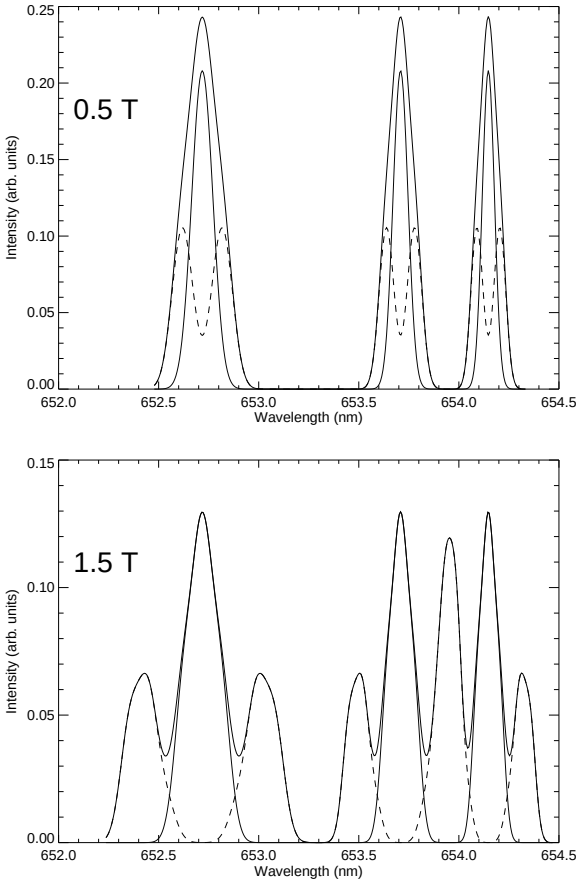

Figure 5. MSE spectra for the model conditions discussed in the text. Key: broken curve—π components; full curve—σ components; thick curve—composite spectrum. The two cases are for magnetic field strengths of 0.5 (top) and 1.5 T (bottom).

Figure 6(a) shows a contour plot of $\zeta_{\mathrm{T}} = (\zeta_\sigma - \zeta_\pi)/2$ against normalized Stark shift $\xi = \Delta\lambda_{\mathrm{S}}/\Delta\lambda_{\mathrm{B}}$ and the normalized delay parameter $\gamma = \phi_0\Delta\lambda_{\mathrm{B}}/\lambda_0$. The maximum ordinate corresponds to a magnetic field of 2.0 T and the maximum abscissa to a delay of 5000 free space wavelengths or a $LiNbO_3$ crystal of thickness $L \sim 40$ mm. The increase in the total spectral width (reduction in temporal coherence) associated with increasing $\Delta\lambda_{\mathrm{S}}$ (increasing B) implies that the normalized delay γ for maximum modulation depth should vary inversely with normalized shift ξ as is evident in the figure. When the delay is too small, the distinction between the equal intensity σ and π components is lost and the contrast modulation disappears. When it is too large, the delay exceeds the temporal coherence for both components and the interference fringes disappear. For small Stark shifts (small ξ) the optimum delay is determined mainly by the spectral width $\Delta\lambda_{\mathrm{B}}$ of each of the component lines.

For comparison with the MOSS spectrometer, we calculate the modulation depth of the light intensity transmitted through a standard filter spectrometer normalized to the amount of light available at the polarimeter as a function of the Stark shift parameter ξ and normalized

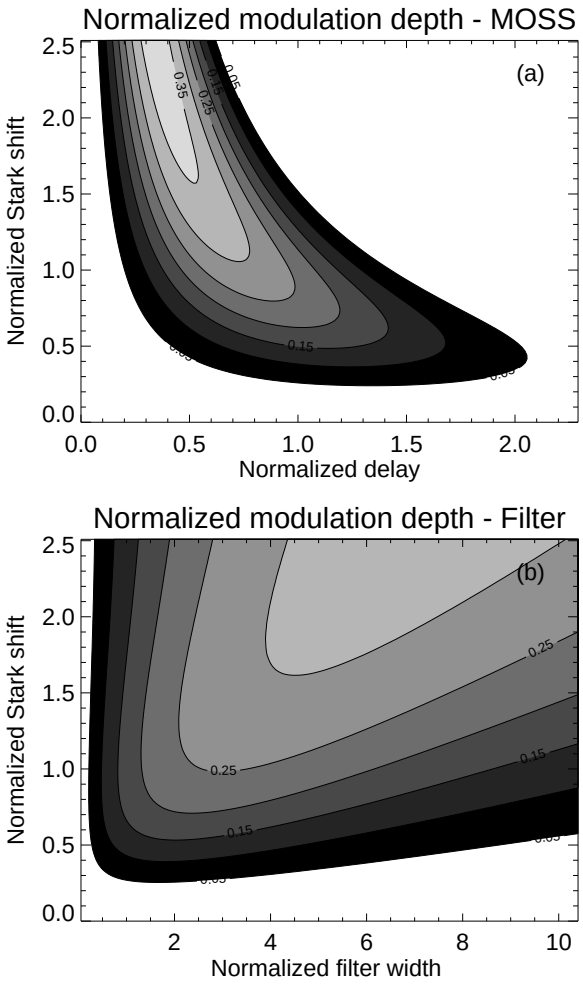

Figure 6. Contour plots of normalized modulation depth (a) ζ_{T} for the MOSS spectrometer and (b) ζ_{F} for the filter spectrometer, as a function of delay parameter and Stark shift normalized to the spectral line width for the MOSS spectrometer. See text for discussion.

filter bandwidth $\Delta\lambda_{\mathrm{F}}/\Delta\lambda_{\mathrm{B}}$. The light transmitted by the filter is given by

$$I_{\mathrm{F}} = \int \mathrm{d}\lambda\, F(\lambda)(\mathcal{I}_\sigma(\lambda)\cos^2\tilde{\psi} + \mathcal{I}_\pi(\lambda)\sin^2\tilde{\psi}) \tag{18}$$

where

$$F(\lambda) = \frac{1}{1 + 4(\lambda - \lambda_0)^2/\Delta\lambda_{\mathrm{F}}^2} \tag{19}$$

is the model Lorentzian filter response having FWHM $\Delta\lambda_{\mathrm{F}}$. The maximum depth of modulation of I_{F} is clearly given by

$$\zeta_{\mathrm{F}} = \frac{1}{I_0}\int \mathrm{d}\lambda\, F(\lambda)(\mathcal{I}_\sigma(\lambda) - \mathcal{I}_\pi(\lambda)). \tag{20}$$

In the extreme case, where the outer π components are rejected entirely by the filter, the intensity varies between zero and a maximum I_0 and the filter 'contrast' is $\zeta_{\mathrm{F}} = 1$. In other words,

the maximum modulation amplitude is $I_0\zeta_F/2$ about an average intensity $I_0\zeta_F/2$. This is the same as for the MOSS spectrometer and, as might be expected, there is no inherent advantage of contrast modulation over the filter method in this limit, apart from certain instrumental considerations noted below. Figure 6(b) shows a contour plot of $I_0\zeta_F$. The complementary behaviour to the MOSS spectrometer is immediately evident. As expected, both the filter bandwidth for maximum modulation depth and the modulation depth itself increase with the ratio $\xi = \Delta\lambda_S/\Delta\lambda_B$.

That the MOSS and filter spectrometers exhibit comparable maximum modulation depth as a function of the Stark shift parameter ξ is illustrated in figure 7. As noted earlier, the dependence on ξ for small Stark shifts is quadratic. As ξ increases, the modulation depth for both MOSS and filter spectrometers aproaches the limiting value $I_\sigma/(I_\sigma + I_\pi) \approx 1/2$. The reason for the small difference between the two cases owes probably to the nature of the spectral discrimination offered by the Lorentzian line-shape filter.

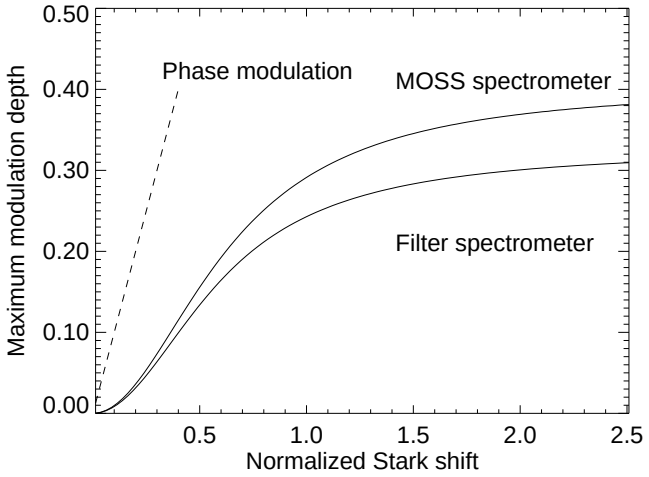

Figure 7. A plot of maximum normalized modulation depth against Stark parameter ξ for both the filter spectrometer and the contrast modulated MOSS spectrometer. See text for discussion.

The principal advantage of the MOSS spectrometer over the interference filter, in this case, is its ready extrapolation to very narrow linewidths. For example, for a magnetic field strength 0.8 T and beam parameters as described previously, we obtain $\Delta\lambda_S \approx \Delta\lambda_B$ for which the optimum filter FWHM is around 0.1 nm. Such extremely narrowband filters are expensive and difficult to manufacture, have poor transmission and require to be carefully tilt or temperature tuned to efficiently isolate the central σ component. A signal to noise improvement of $\sqrt{2}$ can also be obtained by using both transmitted and reflected light from the final polarizer in the MOSS spectrometer. Though, in principle, this light is also available from the component reflected by the interference filter, it is practically much more difficult to realize.

The MOSS spectrometer is a solid-state two-beam interferometer. It is robust against extraneous vibrations and requires minimal alignment. The ease of delay tuning (requiring a change of birefringent plate thickness only) should more easily allow the MSE diagnostic to operate at low magnetic field strengths. When combined with the spherical quadrature polarimeter, the instrument is also sensitive to changes in magnetic field strength (through variations in polarization contrast amplitude) and variations in beam Doppler shift or spectral asymmetry through changes in the interferometer phase offset ϕ_0. However, as in the filter spectrometer case, the minimum measureable field strength is fundamentally limited by the

heating beam divergence through the requirement that $\xi \gtrsim 1$ for reasonable polarization contrast.

4.2. Hybrid scheme

Assuming that the full multiplet is spectrally isolated from the background, a particularly simple hybrid scheme is to replace the second phase plate of the polarimeter with an extended birefringent plate. This results in both a relative change in the visibility of σ and π components as well as a variable phase delay for the purposes of polarimetric discrimination. The polarization change depends on $\Delta\lambda_S$ since the birefringent phase lag δ_2 is wavelength dependent. The arrangement that might be employed in an imaging system is shown schematically in figure 8.

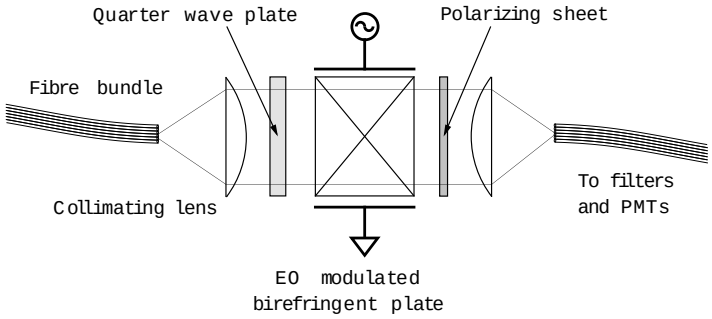

Figure 8. A schematic diagram of the coherence sensitive polarimeter described in the text.

Ignoring ellipticity and by analogy with equations (4) and (5), the total signal is

$$\begin{aligned} 2P_{\pm}(\lambda) = {\sum_{n\geqslant 0}}' I_{\sigma}^{(n)} \left(1 \pm \zeta_B \cos\left(2\psi - \phi_0 - \phi_0 n \frac{\Delta\lambda_S}{\lambda_0}\right)\right) \\ + \frac{1}{2}\sum_{m>0} I_{\pi+}^{(m)} \left(1 \mp \zeta_B \cos\left(2\psi - \phi_0 - \phi_0 m \frac{\Delta\lambda_S}{\lambda_0}\right)\right) \\ + \frac{1}{2}\sum_{m>0} I_{\pi-}^{(m)} \left(1 \mp \zeta_B \cos\left(2\psi - \phi_0 + \phi_0 m \frac{\Delta\lambda_S}{\lambda_0}\right)\right) \qquad (21) \\ = \mathcal{I}(\lambda)(1 \pm \zeta_P(\lambda)\cos(2\psi - \phi_0 - \delta \sin\Omega_P t)) \qquad (22) \end{aligned}$$

where $\pi(\pm)$ denote the upper and lower wavelength subsets of the π group of lines, ϕ_0 is given by equation (8) and the wavelength-dependent polarimetric contrast is

$$\zeta_P = \frac{\mathcal{I}_\sigma \zeta_\sigma - \mathcal{I}_\pi \zeta_\pi}{\mathcal{I}_\sigma + \mathcal{I}_\pi} \qquad (23)$$

with component contrasts given by equation (15) and its equivalent for the π set. The offset delay ϕ_0 is electro-optically modulated with amplitude $\delta = \pi/2$ at Ω_P. This generates signal components at harmonics of Ω_P, the relative amplitudes of which yield the total phase $2\psi - \phi_0$.

Assuming equal intensity σ and π components, the coherence-polarimeter contrast ζ_P is identical to ζ_T for the contrast sensitive polarimeter/interferometer described in section 4.1. There is an inherent S/N advantage for the hybrid system in that no light is lost at the intermediate polarizer as in figure 4. Moreover, only a single non-resonantly excited modulating plate is required. However, because ψ and ϕ_0 are coupled in this simple scheme, it would be important that the birefringent plate is thermally stabilized to avoid phase drifts

that could degrade the accuracy of the measurement. Alternatively, changes in the dc phase ϕ_0 could be monitored interferometrically using a laser beam and the drift compensated during data processing.

4.3. Phase modulation

The wavelength dependence of the phase delay ϕ_0 can be exploited to potentially enhance the polarimeter/spectrometer sensitivity to small Stark shifts. To demonstrate this, consider the idealized case where say, the frequency *upshifted* Stark π components were eliminated. The now unbalanced π sidebands will give rise to a modulation of the spectrometer phase. The simplest way to see this is to note that, under these circumstances, the MOSS spectrometer would sense a spectrum whose weighted centre wavelength shifts periodically (at frequency $2\Omega_P$) by $\Delta\lambda = \alpha\Delta\lambda_S$ where $\alpha \approx 3$ is a constant. The associated phase shift (by the accordion effect) is $\Delta\phi = (\Delta\lambda/\lambda_0)\phi_0 = \alpha\gamma(\Delta\lambda_S/\Delta\lambda_B) = \alpha\gamma\xi$.

It can be shown using equation (10) that optimum sensitivity of the MOSS spectrometer to small wavelength changes (for example, due to Doppler effect) is obtained for $\gamma = 1$ (see the appendix). For smaller γ (smaller path delay ϕ_0) the fringe visibility is greater but the phase amplification $\Delta\phi = (\Delta\lambda/\lambda)\phi_0$ is smaller. Conversely, for large γ the fringe visibility decreases along with the signal to noise ratio. Setting $\gamma = 1$, the phase modulation associated with the shifting of the spectrum first moment will be

$$\Delta\phi = \alpha\Delta\lambda_S/\Delta\lambda_B = \alpha\xi. \tag{24}$$

Note that this phase shift is *linear* in the small quantity ξ compared with the *quadratic* dependence in the case of contrast modulation.

It is instructive to compare the sensitivity of the contrast and phase modulation techniques for detection of small Stark shifts. It is also shown in the appendix that for $\gamma = 1$, the maximum fractional change in signal intensity $\Delta I/I$ for a small phase shift $\Delta\phi$ is given by $\Delta I/I = \exp(-1/2)\Delta\phi$. This establishes the link between the contrast modulation technique (which relies on sensing the modulation $\Delta I/I$) and the phase sensitive method. Substituting for $\Delta\phi$ from equation (24) verifies the linear relationship (valid for small $\Delta\phi$) between the minimum measureable Stark shift ξ and the intensity resolution $\Delta I/I$ (determined by the light signal to noise ratio) in the case of phase sensitive detection:

$$\Delta I/I = g\xi \tag{25}$$

where $g = \exp(1/2)\alpha \approx 0.6\alpha$. Recall that α is the weighted shift of the Stark multiplet resulting from the introduced spectral asymmetry.

In a practical instrument, this weighting might be achieved by transmitting the σ light and one of the π sidebands through a narrowband interference filter. The resulting shift will depend on the filter response and the factor g must be estimated numerically. However, this factor itself may depend on ξ and the advantage suggested by equation (25) is lost.

For the hybrid scheme proposed in section 4.2, the wavelength dependence of the birefringent phase delay gives rise to a transmitted light signal whose spectral centre of mass can be varied by modulating the phase offset ϕ_0. This is easily seen upon inspection of equation (21) for the response to the upper and lower π subsets. The spectral asymmetry is proportional to $\sin\phi_0 \sin(\phi_0\Delta\lambda/\lambda_0)$ which is of first order in the Stark parameter $\xi\lambda = \phi_0\Delta\lambda_S/\lambda_0$. In this case, a combined polarimeter/interferometer system will produce intensity modulations only to second order in ξ.

5. Discussion

These considerations suggest the following experimental possibilities. In low-field compact torus configurations, the 1/2 and 1/3 energy components should be well separated (see figure 5). Provided the divergence of the half-energy component is not too great, there may be the opportunity to simultaneously measure the electric field orientation at different beam velocities and so recover that component due to the motional Stark effect alone. Conversely, in the plasma edge region, where the MSE emission is brightest and the magnetic field is relatively well known, it may be possible to use full and half energy emissions to estimate the plasma electric field. This is certainly the case in stellarators which can exhibit quite high electric fields in the plasma edge region. It must be borne in mind, however, that for fields approaching 1000 V cm^{-1} (a 50 kV deuterium beam at 0.1 T generates 2100 V cm^{-1}), the hyperfine splitting is comparable with the Stark effect [13] and must be considered when modelling the system response.

In conclusion, the instrumental methods proposed here offer the possibility for increased low-field sensitivity for motional Stark effect diagnostic systems. This will be extremely important for future generation low-aspect ratio devices. The possibility for edge electric field measurements in stellarator devices is also noted.

Appendix. MOSS spectrometer sensitivity

We rewrite equation (10) in the notationally simpler form

$$2P = I\{1 \pm \zeta_{\mathrm{B}} \cos((1+\beta)\phi_0)\} \tag{26}$$

where we have ignored the periodic phase modulation ϕ_{M} and have included the possibility of spectrometer phase changes through the factor β. For example, in the case of a Doppler shift of the line centre frequency we have $\beta = v/c$. The maximum sensitivity to variations in β is given by

$$S \equiv \max\left(\frac{\partial P}{\partial \beta}\right) = I\phi_0\zeta_{\mathrm{B}} \tag{27}$$

where the visibility ζ_{B} is a function of ϕ_0 through equation (11). The phase offset ϕ_0 for maximum sensitivity S is is found by differentiation with respect to ϕ_0 to be given by the condition $\gamma = \phi_0(\Delta\lambda_{\mathrm{B}}/\lambda) = 1$ (or $T_{\mathrm{B}} = T_{\mathrm{C}}/2$) where $\Delta\lambda_{\mathrm{B}}$ is the line spectral width. With this condition and noting that the change $\Delta\beta$ gives an associated phase change $\Delta\phi = \phi_0\Delta\beta$, we find using equation (27) that the maximum fractional intensity change accompanying this phase variation is

$$\frac{\Delta I}{I} = \exp(-1/2)\Delta\phi. \tag{28}$$

For the phase sensitive MSE system proposed here we use equation (24) to obtain

$$\frac{\Delta I}{I} = \exp(-1/2)\Delta\lambda_{\mathrm{S}}/\Delta\lambda_{\mathrm{B}} \tag{29}$$

which is linear in the Stark shift $\Delta\lambda_{\mathrm{S}}$.

References

[1] Levinton F M *et al* 1989 *Phys. Rev. Lett.* **63** 2060
[2] Levinton F M *et al* 1990 *Rev. Sci. Instrum.* **61** 2914
[3] Wroblewski D *et al* 1990 *Rev. Sci. Instrum.* **61** 3552

[4] Wroblewski D and Lao L L 1992 *Rev. Sci. Instrum.* **63** 5140
[5] Rice B W 1997 *Fusion Eng. Design* **34–35** 135
[6] Xu J, Ida K, Fujita J and Toi K 1997 *Fusion Eng. Design* **34–35** 297
[7] Howard J 1998 *Rev. Sci. Instrum.* in preparation
[8] Australian Scientific Instruments A Division of Anutech Pty Ltd, phone: 61 2 6280 7570, Fax: 61 2 6280 4985. Contact John.Hyder@asi.anutech.com.au
[9] Hinds Instruments, 3175 NW Aloclek Drive, Hillsboro, OR 97124-7135, USA
[10] Howard J 1995 *Rev. Sci. Instrum.* **66** 383
[11] Xu J *et al* 1997 *Fusion Eng. Design* **34–35** 293
[12] Hamberger S M, Blackwell B D, Sharp L E and Shenton D B 1990 *Fusion Technol.* **17** 123
[13] Bethe H A and Salpeter E A 1957 *Quantum Mechanics of One- and Two-Electron Atoms* (Berlin: Springer)